Fau *et al. Epigenetics & Chromatin* (2026) 19:26
https://doi.org/10.1186/s13072-026-00677-y

Epigenetics & Chromatin

RESEARCH Open Access

Temporal stratification of promoter-proximal versus enhancer VDR binding directs vitamin D-responsive transcription

Priman Alfred Fau[1], Antonio Neme[2], Sabine Seuter[3,4] and Carsten Carlberg[1,3*]

Abstract

Background The active vitamin D metabolite 1,25-dihydroxyvitamin D_3 ($1,25(OH)_2D_3$) activates the vitamin D receptor (VDR) in immune cells, altering the epigenome to drive diverse responses. However, how the temporal dynamics, genomic positioning, and inducibility of VDR binding are integrated to determine transcriptional outcomes remains incompletely understood.

Results Here, we present a time-resolved analysis of VDR-mediated gene regulation in human THP-1 monocytes, integrating VDR ChIP-seq profiles at 40 min, 4, 8, and 24 h with matched transcriptome data following stimulation with $1,25(OH)_2D_3$. Time-resolved VDR ChIP-seq revealed > 22,000 binding sites, with > 5,100 showing ligand-inducible occupancy that expanded over time. This expansion parallels a marked increase in vitamin D-responsive genes, evolving from a limited early response to a broad late transcriptional program. Using distance- and topologically associated domain-informed assignment strategies, we classify vitamin D target genes according to their spatial and temporal association with VDR binding, distinguishing promoter-proximal and enhancer-dominated regulatory architectures. Early vitamin D target genes are characterized by frequent VDR occupancy at transcription start site regions, often supported by coordinated enhancer binding, whereas late-responsive genes are predominantly associated with distal enhancers or lack assignable VDR-driven regulatory models. Importantly, promoter-proximal VDR binding is consistently stronger and more inducible than enhancer-only binding and is associated with higher basal expression and greater transcriptional responsiveness.

Conclusions Together, these findings define a hierarchical, multi-layered model of vitamin D signaling in which early, promoter-proximal VDR binding is strongly associated with establishment of a transcriptionally competent core program, while later enhancer-mediated and indirect mechanisms progressively expand and diversify the response.

Keywords VDR cistrome, Temporal dynamics, ChIP-seq, THP-1 monocytes, Enhancer-Promoter

*Correspondence:
Carsten Carlberg
c.carlberg@pan.olsztyn.pl
[1]InLife Institute of Animal Reproduction and Food Research, Polish Academy of Sciences, ul. Trylińskiego 18, 10-683 Olsztyn, Poland
[2]Instituto de Investigaciones en Matemáticas Aplicadas y en Sistemas, Universidad Nacional Autónoma de México, Mexico City, Mexico
[3]Institute of Biomedicine, University of Eastern Finland, Kuopio, Finland
[4]Present address: Fachbereich Medizin, Dekanat, Goethe Universität, Frankfurt am Main, Germany

Background

Vitamin D, a vital micronutrient obtained from skin UV-B exposure, diet, or supplements [1, 2], maintains calcium homeostasis for bone mineralization and modulates immunity [3, 4]. It bolsters antimicrobial defenses against pathogens [5] while curbing excessive inflammation in autoimmune diseases [6], with prior immune challenges epigenetically priming these responses [7]. These effects stem from the active vitamin D metabolite $1,25(OH)_2D_3$ [8–10], which potently activates the transcription factor VDR [11–13]. VDR is a member of the nuclear receptor superfamily [14], which in humans encompasses 48 receptors, many of which respond to small, lipophilic ligands [15]. Despite differences in ligands and target genes, the fundamental chromatin-based mechanisms of nuclear receptor signaling are largely conserved across the superfamily [11, 16]. For VDR, the canonical model describes binding to DNA at direct repeat (DR3) motifs, which are two hexameric sequences separated by three nucleotides, where VDR forms heterodimers with the retinoid X receptor (RXR) [17].

Genome-wide chromatin immunoprecipitation sequencing (ChIP-seq) has extensively mapped the VDR cistrome in multiple in vitro systems, including THP-1 monocytic leukemia cells [18]. Despite extensive mapping of the VDR cistrome, it remains unclear how the temporal dynamics, genomic positioning, and inducibility of VDR binding are integrated to determine the hierarchy, strength, and timing of vitamin D-dependent transcriptional responses. In particular, whether promoter-proximal and enhancer-mediated VDR binding represent functionally distinct regulatory modes has not been systematically addressed. Previous analyses have identified more than 10,000 potential VDR binding sites [19], but only a subset, typically a few hundred, are consistently occupied across different cellular contexts [20]. Moreover, comprehensive profiling across six human cellular models revealed that only approximately 11% of the mapped sites contain a DR3 motif beneath their binding summit [19]. This observation suggests that VDR employs additional mechanisms for genomic targeting, including cooperative interactions with other nuclear proteins or indirect "piggybacking" on transcription factors already bound to DNA [21–23].

VDR is expressed in nearly all human tissues, with the notable exception of the brain (as indicated by GTEx data [24]), and regulates hundreds of genes in a tissue- and individual-specific manner [25, 26]. Upon ligand binding, the receptor undergoes a conformational change in its ligand-binding domain, which modifies the protein surface and facilitates interactions with coactivators and corepressors [27]. These coregulatory proteins assemble into larger complexes with chromatin-modifying enzymes such as histone acetyltransferases and deacetylases [28]. The coordinated activity of these complexes results in transient chromatin remodeling at enhancer and transcription start site (TSS)/core promoter regions, ultimately enabling gene transcription [29].

Our chromatin-centered model proposes that VDR-bound enhancers preferentially influence genes within the same topologically associated domain (TAD) [30, 31], although enhancer-promoter relationships are probabilistic and may involve multiple regulatory configurations [32]. TADs, which typically range from 100 kb to 2 Mb [33], provide the structural framework for enhancer-promoter interactions, ensuring spatially confined and context-dependent transcriptional responses to vitamin D signaling. Changes in the transcription of primary target genes therefore reflect VDR-mediated remodeling of the epigenome. Based on CTCF (CCCTC-binding factor) HiChIP and high-throughput chromosome conformation capture (Hi-C) approaches in THP-1 cells VDR activation was found to induce selective, functionally relevant changes in 3D chromatin interactions, including altered promoter-enhancer looping and modulation of TAD boundaries [32]. Importantly, vitamin D target genes were enriched within ligand-responsive chromatin loops, supporting a model in which VDR signaling reshapes spatial genome organization to fine-tune transcriptional responses. However, integration of VDR binding dynamics, position, and inducibility to shape transcription remains unclear.

In this study, we examine the spatiotemporal dynamics of VDR binding in THP-1 monocytes over a 40-min to 24-h period and integrate these data with a corresponding transcriptome time course in the same cellular model. We hypothesize that early, promoter-proximal VDR binding establishes a transcriptionally competent primary gene program, whereas later, enhancer-dominated VDR binding primarily contributes to secondary and indirect regulatory responses.

Results

Temporal stratification of the VDR cistrome in THP-1 monocytes

THP-1 monocytes were treated in three biological replicates with either $1,25(OH)_2D_3$ or vehicle control (EtOH) for 40 min, 4 h, 8 h, or 24 h (Figure S1A, left). Following stimulation, the cells were harvested for VDR ChIP-seq analysis. Although the 24-h dataset had been reported previously [20], it was reanalyzed here together with data from three newly generated earlier time points. Across all four time points, we identified 22,469 VDR binding regions (Table S1), representing an expansion of 11,175 sites compared with our previous analysis [20] (Figure S1B).

Comparative analysis of peak intensities across time points and treatment conditions revealed a progressive increase in VDR binding, with maximal occupancy observed after 24 h of $1,25(OH)_2D_3$ stimulation (Fig. 1A). Applying a minimal binding strength threshold (average signal > 50 in at least one sample) refined the VDR cistrome to 9,259 robust binding sites (Table S1). Of these, 5,096 genomic regions displayed significant (false discovery rate (FDR) < 0.05) changes in VDR occupancy upon $1,25(OH)_2D_3$ treatment. The number of ligand-responsive VDR binding sites increased progressively over time, with a pronounced expansion between 8 and 24 h (Fig. 1B, Table S2). Notably, 852 persistent VDR sites were significantly regulated at all four time points, while

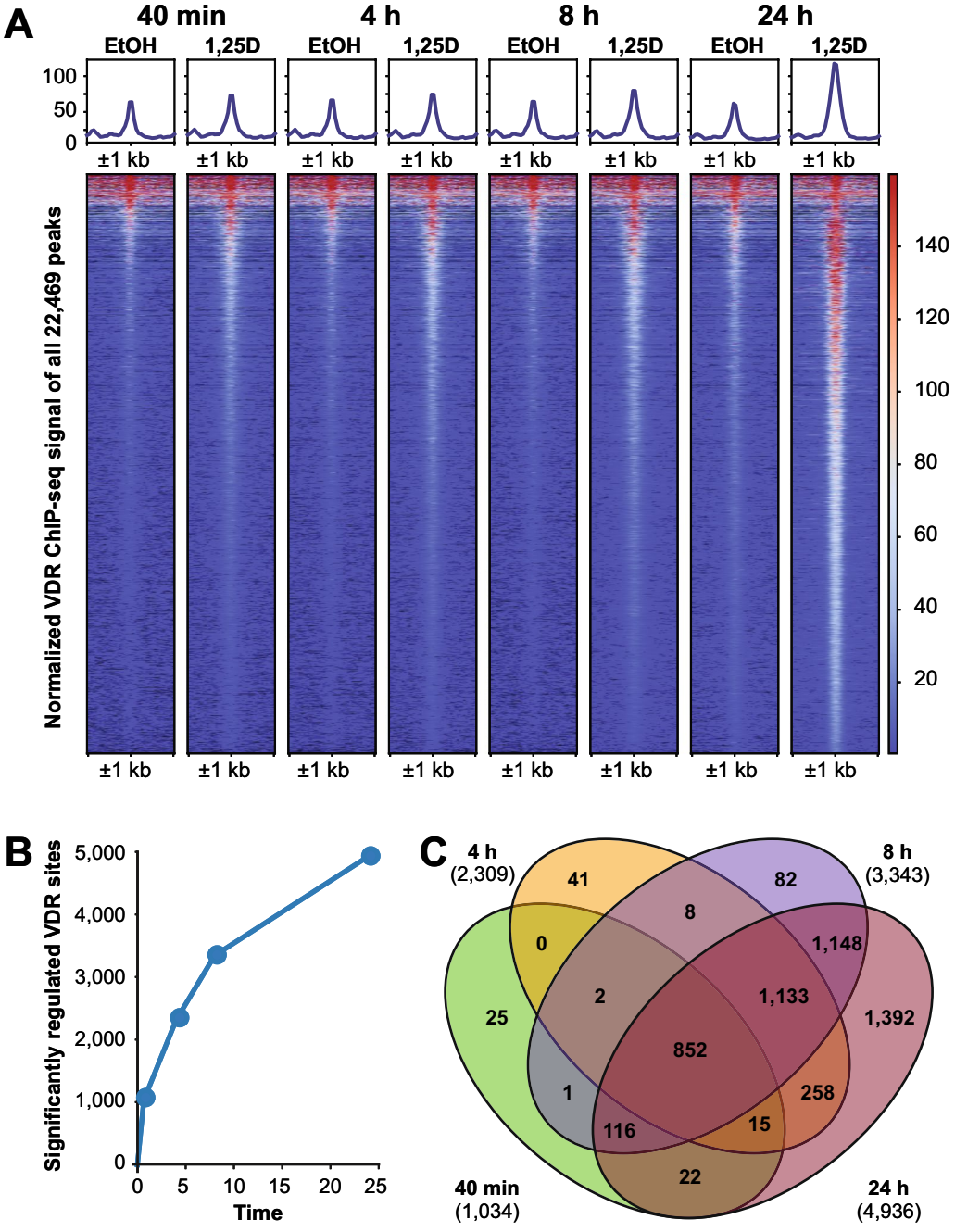

Fig. 1 Temporal dynamics of the VDR cistrome. Heatmaps of normalized VDR ChIP-seq signals (±1 kb from peak centers) across 22,469 VDR binding sites at four time points (40 min, 4 h, 8 h, and 24 h) under ethanol (EtOH, vehicle control) or $1,25(OH)_2D_3$ (1,25D) treatment (**A**). Number of significantly ligand-responsive (FDR < 0.05) VDR binding sites plotted over time (**B**). Venn diagram showing the overlap of significantly regulated VDR sites across time points (**C**)

25, 41, 82, and 1,392 sites were uniquely ligand-sensitive at 40 min, 4 h, 8 h, and 24 h, respectively (Fig. 1C).

Collectively, these data demonstrate that VDR occupancy is progressively established over time and comprises both persistent and temporally restricted binding events.

Temporal coupling of VDR binding dynamics with vitamin D-responsive transcription

To enable direct temporal integration with VDR binding dynamics, we reanalyzed a previously reported RNA-seq dataset generated under matched stimulation conditions [34] (Figure S1A, right). This analysis identified 11,600 expressed protein-coding genes (Table S3), of which 120 were significantly upregulated and 6 downregulated after 2.5 h, 203 (157 up, 46 down) after 4 h, and a markedly larger number, 2,842 genes (1,521 up, 1,321 down), after 24 h of stimulation (Figure S2). These data reveal a pronounced temporal expansion of the vitamin D-responsive transcriptome, encompassing both up- and downregulated genes (Fig. 2A). Notably, 232 genes responded early (within 4 h), while 2,625 genes showed a delayed response to stimulation with $1,25(OH)_2D_3$ (within 4–24 h, Fig. 2B).

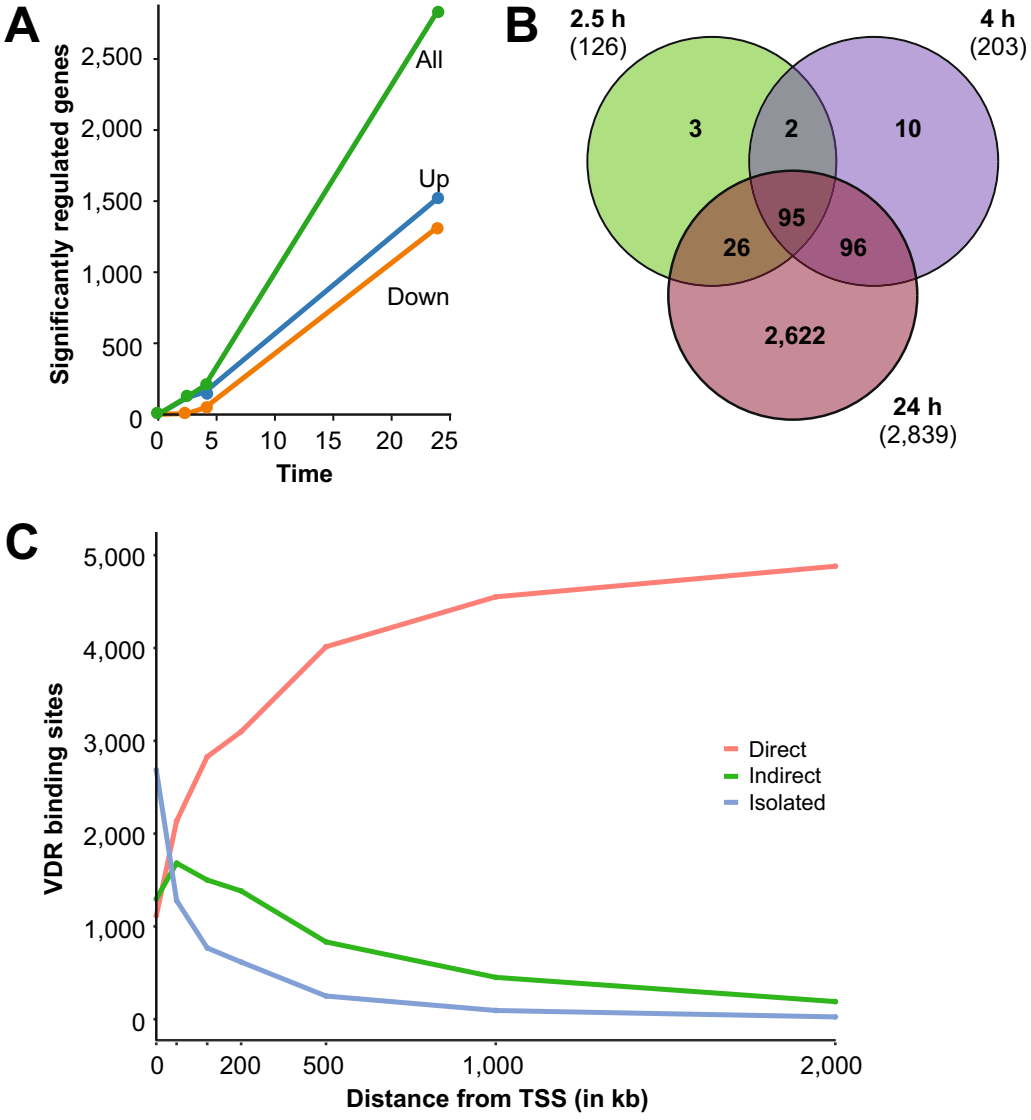

Fig. 2 Time-dependent expansion of the vitamin D-responsive transcriptome and classification of VDR binding sites. Number of significantly regulated protein-coding genes ($p_{adj} < 0.05$) in THP-1 cells following stimulation with $1,25(OH)_2D_3$ for 2.5, 4, and 24 h, shown for all regulated genes (green), upregulated genes (blue), and downregulated genes (orange) (**A**). Venn diagram illustrating the overlap of significantly regulated genes at 2.5, 4, and 24 h of $1,25(OH)_2D_3$ treatment (**B**). Numbers in parentheses indicate the total number of regulated genes at each time point. Classification of significantly ligand-responsive VDR binding sites according to their genomic distance from TSS regions (**C**). VDR sites are categorized as direct (associated with at least one vitamin D target gene), indirect (near a TSS of a non-responsive gene), or isolated (lacking nearby TSS regions), plotted as a function of increasing distance from the TSS

To integrate VDR binding with transcriptional output, we systematically analyzed the spatial relationship between VDR binding sites and TSS regions of nearby genes using distance thresholds of 0 kb (TSS), ± 60 kb, ± 150 kb, ± 200 kb, ± 1 Mb, and ± 2 Mb (Table S4). For each of the seven distances we classified VDR binding sites as *direct* (proximal to one or more vitamin D target genes), *indirect* (proximal exclusively to non-responsive genes), or *isolated* (lacking nearby TSS regions), thereby distinguishing putative regulatory from non-regulatory binding events.

At a distance of 0 kb, corresponding to binding directly at the TSS region, the full set of 5,096 significant VDR sites was partitioned into 1,114 direct, 1,296 indirect, and 2,686 isolated sites (Fig. 2C). Accordingly, 52.7% of all VDR binding sites are located outside TSS regions. With increasing TSS distance, the number of direct sites progressively increased, reaching 4,881 at a distance of 2 Mb, whereas the number of isolated sites declined to 25. In contrast, indirect VDR sites peaked at 2,136 at a distance of 60 kb and subsequently decreased to 190 at 2 Mb.

Time-resolved analysis revealed that at the TSS region (0 kb) the number of direct VDR sites increased from 251 at 40 min to 546, 775, and 1,089 at 4, 8, and 24 h, respectively, and similarly expanded with increasing TSS distance (Figure S3). Indirect and isolated VDR sites displayed comparable proportional dynamics across time points.

Together, these analyses indicate that the temporal expansion of the VDR cistrome is tightly paralleled by an expanding transcriptional response, consistent with a hierarchical regulatory process.

TAD-constrained assignment delineates primary and secondary vitamin D target genes

Given that TADs typically span approximately 1 Mb [33], we focused on a VDR site-to-TSS distance of ± 500 kb as a biologically grounded assignment window (Fig. 3A). Under this criterion, 2,145 (75.2%) of all vitamin D target genes are associated with one or more of the 4,013 direct VDR binding sites, which are likely located within the same TAD (Table S4). These genes were therefore classified as primary vitamin D target candidates based on spatial association with VDR binding. The remaining 709 regulated genes are classified as secondary vitamin D targets, as they are located in TADs that do not contain a VDR binding site. Notably, these proportions closely mirror previous hierarchical estimates obtained using independent analytical strategies [35]. In addition, 833 ligand-modulated VDR binding sites are located close to 655 genes that do not respond transcriptionally to $1,25(OH)_2D_3$. Finally, 250 VDR sites are classified as isolated, as they are too distant from any protein-coding gene to plausibly exert regulatory effects.

Further characterization of VDR binding dynamics showed that 661 direct and 140 indirect VDR sites are persistent, being occupied at all four analyzed time points (Fig. 3B and C). Moreover, 1,925 direct VDR sites are bound at early time points (40 min and 4 h), whereas 2,088 sites are occupied exclusively at later time points (8 and 24 h), indicating substantial temporal remodeling of the VDR cistrome.

Analysis of VDR-TSS distances at 0 kb, ± 60 kb, ± 150 kb, ± 200 kb, ± 1 Mb, and ± 2 Mb (Figure S4) revealed that direct binding to TSS regions (0 kb) involves 1,114 VDR sites regulating 706 primary vitamin D target genes. Of these sites, 586 are bound early and 528 only at later time points. In contrast, 941 genes that do not respond to vitamin D stimulation harbor a total of 1,296 indirect VDR sites at their TSS regions.

The distance threshold of 150 kb is of particular interest, as 158 kb has been reported as the median distance between enhancers and their target TSS regions [36]. At this distance, 2,828 direct VDR sites (1,368 early and 1,460 late) are related to 1,571 primary vitamin D target genes, whereas 1,283 genes would be classified as secondary targets. Under these conditions, 1,118 non-vitamin D-target genes are located near 1,500 indirect VDR binding sites.

In aggregate, TAD-constrained assignment reveals that most vitamin D target genes are directly associated with VDR binding, while a substantial minority, particularly among late-responsive genes, are regulated indirectly.

Temporal coordination of promoter-proximal and enhancer-mediated VDR binding distinguishes early and late vitamin D responses

Among the 232 early vitamin D target genes, more than half (52.2%) exhibit direct VDR occupancy at their TSS regions (Fig. 4A). Of these, 71 show early VDR occupancy and 50 display VDR binding only at later time points. Depending on the maximal distance considered for VDR-bound enhancers, regulatory scenarios could be assigned to an additional 99 genes. Focusing on the ± 500 kb VDR-TSS distance, 48 of the early VDR-occupied TSS regions are supported by an early VDR-bound enhancer and 23 by a late-bound enhancer. Conversely, among the late VDR-occupied TSS regions, 13 are supported by early enhancers and 37 by late enhancers. In addition, under this distance constraint, 82 early vitamin D target genes are regulated exclusively via VDR-bound enhancers, of which 39 are associated with early and 43 with late enhancer occupancy. Nevertheless, even within the ± 500 kb framework, a subset of early vitamin D target genes (n = 29) lacks an assignable VDR-driven regulatory model. HOMER (Hypergeometric Optimization of Motif EnRichment) [37] analysis of ± 50 bp regions centered on VDR ChIP-seq peaks at promoters (TSS regions)

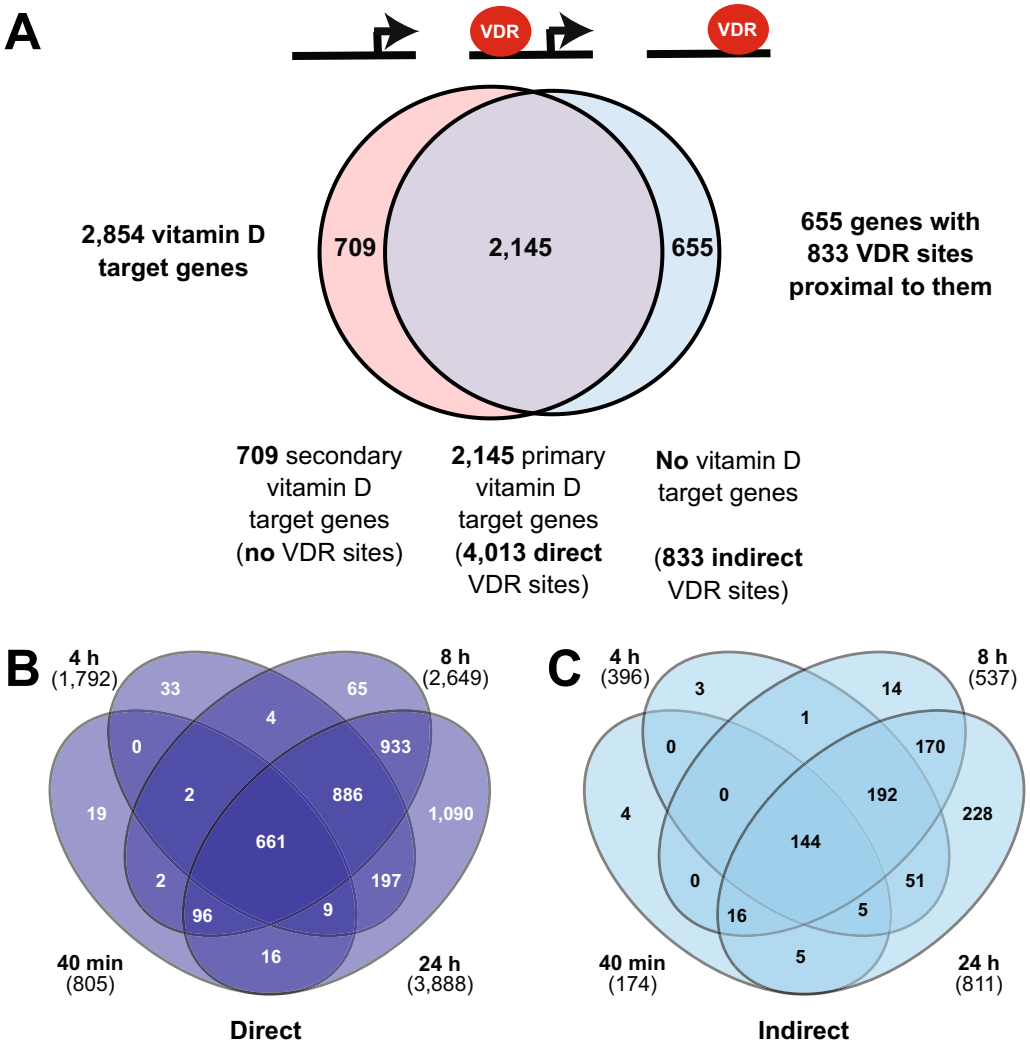

Fig. 3 TAD-constrained assignment defines primary and secondary vitamin D target genes and reveals temporal classes of VDR binding. Classification of vitamin D target genes based on proximity to ligand-dependent VDR binding sites within a ± 500 kb window (**A**). Of the 2,854 vitamin D target genes, 2,145 are classified as primary targets associated with 4,013 direct VDR binding sites, whereas 709 genes lack nearby VDR binding and are defined as secondary targets. In addition, 833 indirect VDR binding sites are located near to 655 non-vitamin D-target genes. Venn diagram showing the overlap of direct VDR binding sites across the four stimulation time points (40 min, 4 h, 8 h, and 24 h), highlighting persistent, early, and late VDR occupancy (**B**). Numbers in parentheses indicate the total number of direct VDR sites detected at each time point. Corresponding Venn diagram for indirect VDR binding sites across the same time points, illustrating their temporal distribution and persistence (**C**)

and enhancers identified DR3-type VDR-RXR motifs as the top-ranked binding sites. However, these motifs were present in only 7.0% of TSS-associated genes and 9.5% of enhancer-only-associated genes. However, when the window size is increased to ± 150 bp the VDRE rate increased to 20.1% and 28.5%, respectively (Figure S5). With lower significance binding motifs for the nuclear receptors NR2F6 (also called EAR2), NR2F1 (also called COUP-TF), THRB (thyroid hormone receptor beta, also called NR1A2) and RARA (retinoic acid receptor alpha, also called NR1B1) were identified. This comparison illustrates the robustness of motif detection across different analytical window sizes and gene set definitions, and highlights distinct regulatory architectures between promoter-proximal and enhancer-mediated early transcriptional responses.

Only 22.3% of the 2,622 late vitamin D target genes are associated with VDR occupancy at their TSS regions (Fig. 4B). Among these, 281 genes display early-responding TSS regions, whereas 304 respond only at later time points. Within the ± 500 kb framework, 201 of the early TSS regions are supported by early VDR-bound enhancers and 80 by late enhancers. Conversely, among late-responding TSS regions, only 80 are supported by early enhancers, while 224 are supported by late enhancers. Moreover, regulatory scenarios for an additional 1,357 late vitamin D target genes can be inferred from enhancer-only models involving 612 early and 745 late

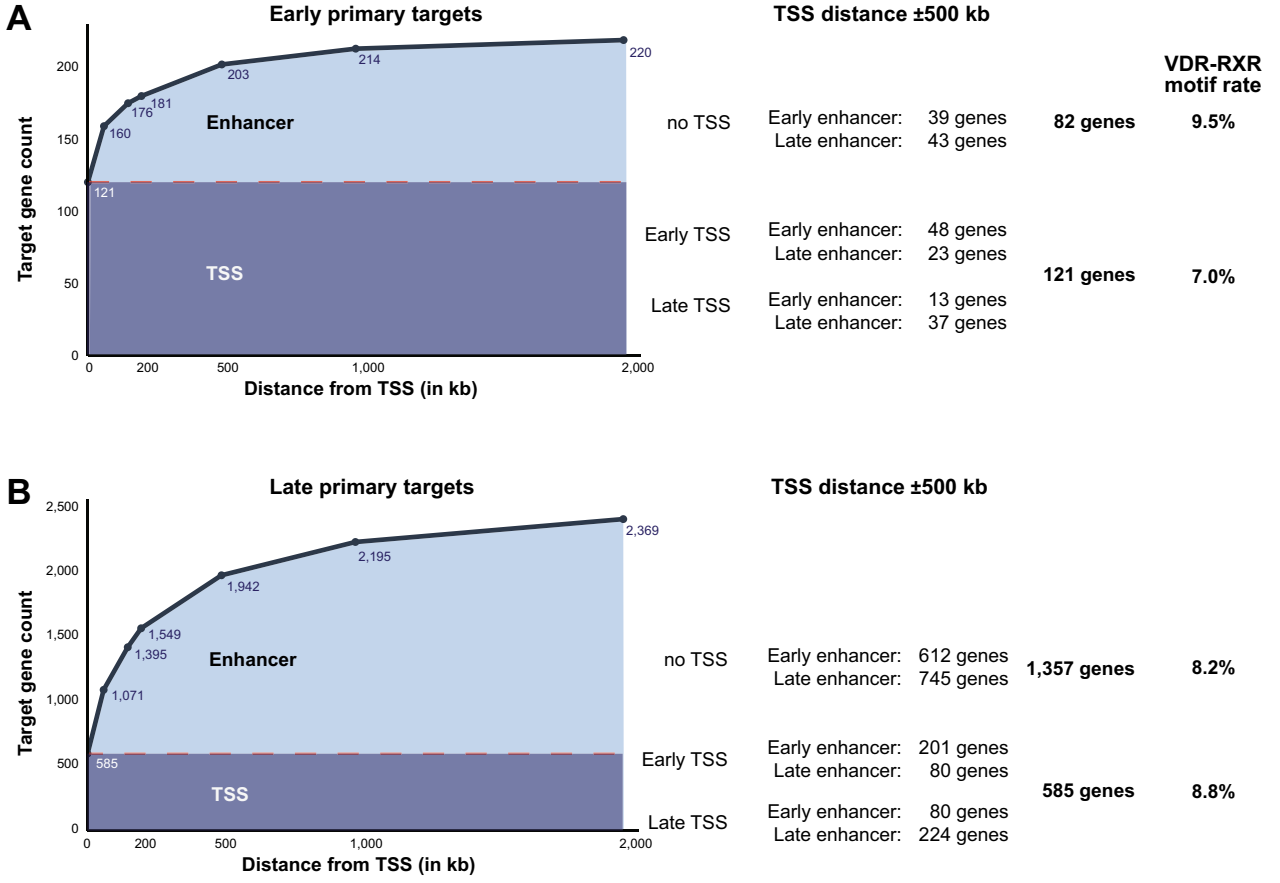

Fig. 4 Temporal coordination of VDR binding at promoters and enhancers distinguishes early and late vitamin D target genes. Distribution of early primary vitamin D target genes as a function of VDR binding relative to TSS regions and enhancers within windows ranging from 0 kb to 2 Mb (**A**). For the example of the ± 500 kb regulatory scenario early targets are stratified into genes with VDR binding at the TSS (early or late TSS occupancy) or genes regulated exclusively via VDR-bound enhancers. Corresponding analysis for late primary vitamin D target genes using the same ± 500 kb distance criterion (**B**). HOMER motif analysis identified DR3-type VDR-RXR binding sites as the top-ranked motifs, with the indicated percentages

VDR-bound enhancers. Collectively, this analysis leaves 680 late vitamin D target genes without an assignable VDR-driven regulatory model, indicating that they are likely secondary vitamin D targets. Consistent with previous analyses [19], HOMER motif analysis (± 50 bp) identified DR3-type VDR-RXR motifs as the top-ranked binding sites, occurring in 8.8% of TSS-associated genes and 8.2% of enhancer-only-associated genes. At a window size of ± 150 bp the VDRE rates are 25.8% and 25.4%, respectively (Figure S5).

Collectively, these analyses show that early vitamin D responses are frequently associated with promoter-proximal VDR occupancy, whereas late responses are dominated by distal enhancer-mediated and indirect regulatory mechanisms.

Promoter-proximal VDR binding confers high-amplitude and early transcriptional responsiveness

The increase in VDR binding strength was compared between TSS and enhancer binding sites. Notably, ligand-induced VDR occupancy at early binding sites was consistently stronger and more inducible at TSS regions than at enhancers across all time points (Fig. 5A). In contrast, at late-responding VDR sites, a significantly higher VDR binding strength at TSS regions compared with enhancers was observed only after 24 h of stimulation with $1,25(OH)_2D_3$ (Fig. 5B). Representative examples include the *CAMP* (cathelicidin antimicrobial peptide) gene, which exhibits an early responding TSS region (Figure S6A), the *CD14* (CD14 molecule) gene, characterized by an early responding enhancer and a late responding TSS region (Figure S6B), and the *FBP1* (fructose-bisphosphatase 1) gene, which shows both late responding enhancer and TSS regions (Figure S6C).

At the transcriptome level, early vitamin D target genes displayed significantly higher inducibility at all three analyzed time points (2.5, 4, and 24 h) when regulation involved VDR binding to TSS regions compared with regulation mediated exclusively by enhancers (Fig. 5C). Although the overall inducibility of early vitamin D target genes exceeded that of late responders, late target genes likewise showed higher inducibility in response to

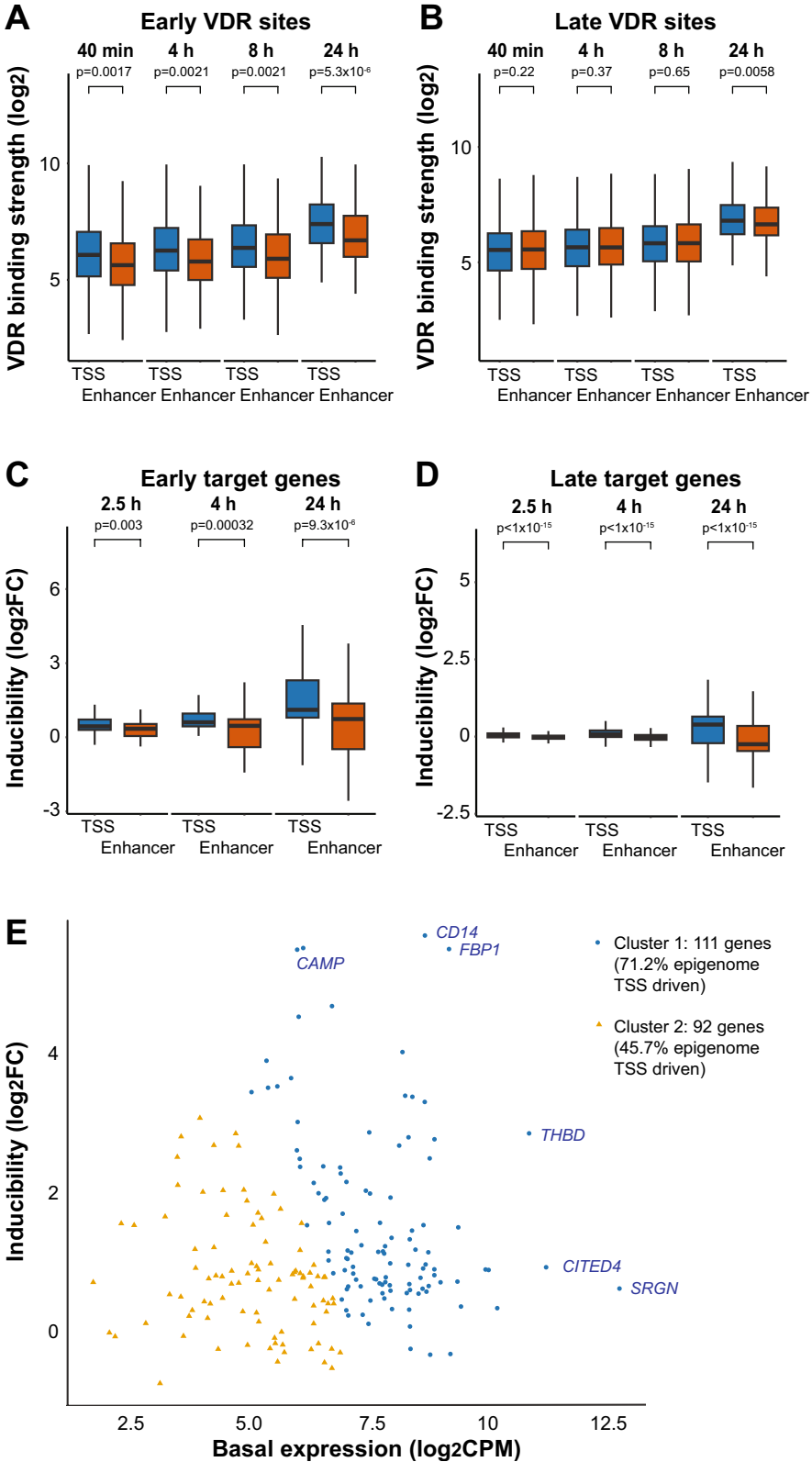

Fig. 5 (See legend on next page.)

(See figure on previous page.)

Fig. 5 Promoter-proximal VDR binding confers stronger inducibility of VDR occupancy and transcriptional responses. Comparison of ligand-induced VDR binding strength at TSS regions and enhancers for early VDR binding sites at 40 min, 4 h, 8 h, and 24 h after stimulation with $1,25(OH)_2D_3$ (**A**). Corresponding analysis for late VDR binding sites, showing significantly higher inducibility at TSS regions compared with enhancers only at 24 h (**B**). Inducibility of early vitamin D target genes at 2.5, 4, and 24 h, stratified by regulation involving TSS-associated VDR binding versus enhancer-only models (**C**). Inducibility of late vitamin D target genes analyzed as in (**C**), demonstrating overall weaker responses but higher inducibility when TSS-associated VDR binding is present (**D**). Relationship between basal gene expression and inducibility for 203 early vitamin D target genes within the ± 500 kb regulatory scenario (**E**). *K-means* clustering identifies two groups: cluster 1, comprising genes with higher basal expression and inducibility, enriched for TSS-driven VDR regulation, and cluster 2, consisting of genes with lower basal expression and inducibility. Selected representative genes are indicated. Box plots show median values with interquartile ranges; whiskers indicate 1.5 × interquartile range. P-values are indicated above comparisons

$1,25(OH)_2D_3$ when driven by TSS-associated VDR binding rather than by enhancers alone (Fig. 5D).

The inducibility of 203 early vitamin D target genes within the ± 500 kb gene regulatory scenario (Fig. 4A) was plotted against their basal expression levels (Fig. 5E). *K-means* clustering identified two distinct groups: cluster 1, comprising 111 genes with higher basal expression and inducibility, and cluster 2, consisting of 92 genes with lower basal expression and inducibility. Importantly, 72.2% (79 genes) of early vitamin D target genes in cluster 1 were driven by vitamin D-inducible VDR binding sites at TSS regions, whereas this proportion was substantially lower in cluster 2 (45.7%, 42 genes).

In summary, promoter-proximal VDR binding emerges as a dominant determinant of both the magnitude and timing of vitamin D-induced transcriptional responses.

Discussion

This study provides a time-resolved dissection of VDR-mediated gene regulation in human THP-1 cells, demonstrating how the temporal dynamics, genomic positioning, and inducibility of VDR occupancy shape transcriptional outcomes. THP-1 cells were selected because they provide a well-established and highly reproducible model for mechanistic dissection of VDR-mediated chromatin regulation [38, 39]. Importantly, their homogeneous epigenetic landscape allows time-resolved integration of ChIP-seq and transcriptome data, which would be difficult to achieve with primary cells due to donor variability and limited material [40]. By integrating ChIP-seq and RNA-seq data across early and late time points, we show that vitamin D signaling is not governed by a static VDR cistrome but by a progressively expanding and functionally stratified regulatory landscape. Building on our previous characterization of the vitamin D-responsive cistrome and chromatin architecture in human monocytes [30, 31, 41], we extend these descriptive frameworks toward a quantitative, hierarchical regulatory model. Whereas earlier models emphasized signal propagation through transcription factor networks and chromatin accessibility [35], the present study demonstrates that the temporal order, genomic location, and inducibility of VDR binding itself are decisive determinants of whether genes respond early, late, or indirectly. In particular, strong and ligand-responsive promoter-proximal VDR binding emerges as a defining feature of early primary target genes, providing a chromatin-based explanation for the initiation of downstream transcriptional cascades.

The progressive expansion of the VDR cistrome reveals that vitamin D signaling is a temporally layered regulatory process in which early VDR binding primes the chromatin landscape for later transcriptional amplification. Although VDR binding is detectable within 40 min, maximal occupancy is reached only after 24 h, indicating that sustained ligand exposure is required to fully establish a vitamin D-responsive chromatin state. These findings support a model of epigenetic priming in which early VDR binding establishes a permissive chromatin state that conditions subsequent transcriptional responsiveness rather than directly dictating transcriptional magnitude [42]. The association of multiple VDR binding sites with higher basal expression supports the concept that VDR preferentially occupies preactive chromatin regions poised for rapid transcriptional response, while ligand stimulation predominantly modulates the amplitude and persistence of transcription rather than initiating widespread de novo gene activation.

Our time-resolved analysis of the VDR cistrome complements and extends previous work on vitamin D-dependent 3D chromatin architecture [32]. The latter focused on ligand-induced changes in CTCF-mediated looping after prolonged stimulation, while our data reveal how dynamic and progressive VDR recruitment to promoters and enhancers precedes and likely drives such higher-order chromatin rearrangements. Together, these findings support a hierarchical model in which early, promoter-proximal VDR binding initiates transcriptional responses, whereas later enhancer-dominated binding contributes to chromatin looping, TAD-internal communication, and indirect gene regulation.

Early transcriptional responses to $1,25(OH)_2D_3$ stimulation are limited in number but highly enriched for direct VDR binding, whereas a large number of late-responding genes are regulated indirectly. This dichotomy reinforces a hierarchical model of vitamin D-dependent gene regulation in which primary target genes are directly controlled by VDR occupancy, whereas secondary targets arise indirectly through VDR-induced transcription

factors, signaling intermediates, or chromatin-modifying enzymes.

By applying TAD-informed distance thresholds, we provide a biologically grounded and chromatin-architecture-consistent framework for assigning VDR binding sites to target genes. Within a ± 500 kb window, consistent with typical TAD dimensions [41], approximately three quarters of all vitamin D target genes can be classified as primary targets. Nevertheless, approximately one quarter of late vitamin D target genes lacks proximal VDR binding even at extended distances, reinforcing the notion that indirect regulatory cascades play a major role, particularly at later stages of the response.

A central conceptual advance is the identification of distinct temporal and spatial patterns of VDR chromatin engagement, reflected in differential enrichment of promoter-proximal versus enhancer-associated binding. Early vitamin D target genes are frequently characterized by direct VDR occupancy at TSS regions, often supported by nearby enhancers, whereas late target genes are predominantly associated with distal enhancer binding and exhibit weaker and delayed transcriptional responses. Importantly, this promoter-proximal VDR binding shows stronger functional association with transcriptional responsiveness than distal binding. These findings indicate that promoter-bound VDR is preferentially observed within transcriptionally permissive chromatin contexts, enabling rapid and robust gene activation. These observations align with Hi-C studies demonstrating that promoters act as central organizational hubs of *cis*-regulatory interactions within topologically associated domains [36], as well as recent high-resolution functional analyses showing that enhancers are selectively constrained by promoter competence and genomic context [43]. In this framework, enhancers do not act uniformly across all genes within a TAD but require productive engagement with competent promoters to exert strong transcriptional effects. This identifies promoter occupancy as a rate-limiting determinant of transcriptional strength and timing.

The relationship between promoter-associated VDR binding, basal gene expression, and inducibility further supports this model. Early vitamin D target genes with high basal expression and strong inducibility are enriched for inducible VDR binding, indicating that preexisting transcriptional activity primes genes for rapid hormonal responsiveness. Conversely, genes with low basal expression and weak inducibility are less frequently associated with inducible VDR binding, suggesting the presence of additional chromatin barriers or regulatory constraints.

This study relies on the THP-1 monocytic cell line, which may not fully capture the heterogeneity or physiological context of primary human immune cells. Nevertheless, the temporal principles identified here are likely conserved across immune cell types. Second, transcriptomic profiling was limited to 2.5, 4, and 24 h, leaving early (40 min) and intermediate (8 h) windows underexplored, which restricts precise temporal integration with VDR binding dynamics. Third, assignment relied on genomic proximity and TAD context rather than direct chromatin conformation measurements. Notably, recent topology-resolved studies indicate that enhancer–promoter relationships are probabilistic and embedded within dynamic transcriptional neighborhoods [32], limiting deterministic assignment even with chromatin interaction data. Finally, this work did not address inter-individual variability, which is an important factor in understanding the diversity of vitamin D responses in vivo.

Conclusion

Our results define a multi-layered model of vitamin D signaling in which early, promoter-proximal VDR binding is strongly associated with rapid activation of a core gene set, while later enhancer-mediated and indirect mechanisms progressively expand the transcriptional response. By integrating temporal VDR binding dynamics with TAD-restricted enhancer-promoter communication and ligand-induced chromatin looping, this framework reconciles promoter-centric and enhancer-driven models of vitamin D action and emphasizes the importance of 3D genome organization for nuclear receptor function. More broadly, our findings position promoter-proximal VDR binding as a key determinant of transcriptional competence and refine the chromatin-based model of vitamin D signaling, providing a generalizable framework for signal-dependent gene regulation by nuclear receptors.

Methods

Cell culture

THP-1 cells, originally derived from the peripheral blood of a 1-year-old male patient with acute monocytic leukemia, were obtained from the American Type Culture Collection (ATCC, TIB-202™) [44]. These cells are a well-established, physiologically relevant model for investigating $1,25(OH)_2D_3$-mediated processes, including innate immunity and cellular growth [45]. Cells were cultured in RPMI 1640 medium supplemented with 10% fetal bovine serum (FBS), 2 mM L-glutamine, 0.1 mg/ml streptomycin, and 100 U/ml penicillin, and maintained at 37 °C in a humidified incubator with 95% air and 5% CO_2. Prior to stimulation, cells were seeded at a density of 0.5×10^6 cells/ml and incubated overnight in phenol red-free medium supplemented with charcoal-stripped FBS. Stimulation was performed for the indicated times with 10 nM $1,25(OH)_2D_3$ (dissolved in ethanol, EtOH) or with 0.1% EtOH as a vehicle control. All experiments were conducted in three biological replicates.

ChIP-seq

ChIP assays were performed as described by Zhang et al. with some modifications [46]. After treatment of 20×10^6 THP-1 cells, nuclear proteins were cross-linked to genomic DNA by adding formaldehyde directly to the medium to a final concentration of 1% and incubating at room temperature for 10 min on a rocking platform. Cross-linking was stopped by adding glycine to a final concentration of 0.125 M and incubating at room temperature for 10 min on a rocking platform. Cells were harvested by centrifugation and washed twice with ice-cold PBS to remove residual medium. The resulting cell pellets were immediately snap-frozen to preserve integrity and stored at – 80 °C.

Before subsequent processing, pellets were thawed slowly on ice. The cell pellets were subsequently resuspended twice in 10 ml cell lysis buffer (0.1% SDS, 1 mM EDTA, 150 mM NaCl, 1% Triton X-100, 0.1% sodium deoxycholate, protease inhibitors, 50 mM HEPES–KOH, pH 7.5) and once in 10 ml nuclear lysis buffer (1% SDS, 1 mM EDTA, 150 mM NaCl, 1% Triton X-100, 0.1% sodium deoxycholate, protease inhibitors, 50 mM HEPES–KOH, pH 7.5). After two washes with cell lysis buffer, the chromatin pellet was resuspended in 700 µl of SDS lysis buffer (1% SDS, 10 mM EDTA, protease inhibitors, 50 mM Tris–HCl, pH 8.1) and the lysates were sonicated in a Bioruptor Plus (Diagenode) to result in DNA fragments of 200–500 bp. Cellular debris was removed by centrifugation. 175 µl aliquots of the lysate were diluted 1:5 in IP dilution buffer (1% Triton X-100, 2 mM EDTA, 150 mM NaCl, protease inhibitors, 20 mM Tris–HCl, pH 7.5). 14 µl anti-VDR antibody (Cell Signaling Technology, #12550) was coated to 35 µl Dynabeads Protein G (Invitrogen) in an overnight incubation at 4 °C. The preformed bead-antibody complexes were then washed twice with beads wash buffer (0.1% Triton X-100, PBS, protease inhibitors) and added to the chromatin aliquots. The samples were incubated overnight at 4 °C on a rotating wheel to form and collect the immuno-complexes.

The beads were washed sequentially for 5 min on a rotating wheel with 300 µl of the following buffers, each: three times cell lysis buffer, once high salt buffer (0.1% SDS, 1% Triton X-100, 1 mM EDTA, 350 mM NaCl, 0.1% sodium deoxycholate, 50 mM HEPES–KOH, pH 7.5), once ChIP wash buffer (250 mM LiCl, 1% Nonidet P-40, 0.5% sodium deoxycholate, 1 mM EDTA, 10 mM Tris–HCl, pH 8.0) and once 10 mM Tris–HCl, pH 8.0. The beads were resuspended in 150 µl of 10 mM Tris–HCl (pH 8.0) and transferred to a new tube. After discarding the supernatant, ChIPmentation [47] was performed by resuspending the beads in 50 µl of tagmentation mix (10 µl 5 × tagmentation buffer [5 mM EDTA pH 8.0, 0.4% SDS, 300 mM NaCl, 50 mM Tris–HCl pH 8.0], 38 µl nuclease-free water, and 2 µl of 1:10-diluted Tn5 transposase [Illumina]). The reaction was incubated at 37 °C for 10 min with gentle mixing after 5 min. Tn5 transposase was subsequently inactivated by adding 300 µl of Cell Lysis Buffer, inverting the tube five times, and incubating on ice for 5 min.

Then the beads were washed sequentially with 300 µl of buffer per step, inverting five times for each wash: twice with Cell Lysis Buffer and twice with TE buffer (10 mM Tris–HCl pH 8.0, 1 mM EDTA). Elution and crosslink reversal were performed by adding 48 µl of ChIPmentation Elution Buffer (10 mM Tris–HCl pH 8.0, 5 mM EDTA pH 8.0, 0.4% SDS, 300 mM NaCl) and 2 µl proteinase K, followed by incubation for 1 h at 55 °C and 4–6 h at 65 °C. A second elution was performed by adding 19 µl of ChIPmentation Elution Buffer and 1 µl proteinase K, incubating for 6–8 h at 55 °C, and combining both eluates.

To determine the optimal number of PCR cycles for library amplification, 2 µl of eluted DNA were used in a 10 µl test PCR with 2 × KAPA HiFi HotStart ReadyMix (Roche). Libraries were then amplified in a 50 µl reaction containing 25 µl 2 × KAPA HiFi HotStart ReadyMix, 2 µl nuclease-free water, and 1.5 µl Nextera custom primer Ad1.noMX (25 µM), preheated at 98 °C for 30 s before adding 20 µl of ChIPmentation DNA and 1.5 µl Nextera custom index primer Ad2.1(-24) (25 µM) [48]. Amplification was carried out using the cycle number determined in the preliminary PCR.

Libraries were purified by right-side size selection using 32.5 µl of Agencourt AMPure XP beads (Beckman Coulter), followed by a second purification with 57.5 µl AMPure XP beads, and eluted in 15 µl of nuclease-free water. Library concentration was quantified using the Qubit dsDNA HS Assay Kit (Invitrogen), and fragment size distribution was assessed using the Agilent Bioanalyzer High Sensitivity DNA Assay.

ChIP-seq analysis

VDR ChIP-seq libraries were sequenced at 50 bp read length using standard manufacturer protocols at the Gene Core of the EMBL (Heidelberg, Germany). All ChIP-seq data (Table S5) were analyzed at harmonized settings: alignment with the human reference genome version hg38 using STAR software version 2.7.2a [49]. Reads overlapping ENCODE blacklist intervals (hg38-blacklist.v2 [50]) were excluded and low quality reads were filtered out using samtools view with the -q 2 parameter. PCR bias was minimized by marking duplicate reads with samtools markdup. Indexed and sorted BAM files were processed for differential binding analysis by using CSAW package version 1.4 [51]. Counts were generated with fragment length 110 and a window with 150 bp and only kept the standard chromosomes. The counts were normalized with composition bias by using

edgeR version 4.4.2 [52], differential binding was assessed for each stimulation time point relative to the vehicle control and aggregate the sliding windows into regions where the VDR binding sites occur. The regions binding were annotated with ChIPseeker version 1.40.0 [53] and TxDb.Hsapiens.UCSC.hg38.knownGene version 3.18.0 package. A significant modulation of VDR ChIP-seq peaks by $1,25(OH)_2D_3$ was computed by comparing the intensity of peaks obtained from ligand-treated THP-1 cells to the colocated peak intensity obtained from vehicle-treated cells. The three independent replicate experiments allowed the calculation of statistical significance (p-value and FDR, Table S1 and Table S2). Motif enrichment analysis for differentially accessible regions was conducted using HOMER software version 5.1 [37].

Transcriptome and differential gene expression analysis

Transcriptome data were obtained from a previous study [34], in which the following protocol was used. Cells were preserved in TRIzol, and total RNA was isolated using the High Pure RNA Isolation Kit (Roche). RNA integrity and concentration were assessed with a Bioanalyzer (Agilent 2100; RNA Nano 6000 Assay). Ribosomal RNA was depleted using the NEBNext rRNA Depletion Kit, and complementary DNA (cDNA) libraries were prepared from the rRNA-depleted RNA with the NEBNext Ultra II Directional RNA Library Prep Kit for Illumina. Library quality was verified with the Agilent DNA 1000 Chip, and indexed libraries were pooled before sequencing. RNA-seq libraries were sequenced on an Illumina NextSeq 500 platform (Illumina) with 75 bp read length, following standard protocols, at the Gene Core facility of EMBL (Heidelberg, Germany) (Table S5).

RNA-seq data were reprocessed using the latest human genome assembly and corresponding gene annotation. Single-end, reverse-stranded cDNA sequence reads were checked by using FastQC for the quality control. Read then aligned to the GRCh38 reference genome (GENCODE release 43) using the STAR aligner version 2.7.2a. Read quantification was performed with FeatureCounts version 2.0.6 [54]. Gene annotation, including Ensembl gene identifiers, gene symbols, descriptions, genomic locations, biotypes, and Entrez Gene IDs, was carried out using the Ensembl database (release 110) via the BiomaRt R package version 2.62.1 [55]. Samples with read counts below 10 were discarded, and only protein coding genes were kept for the downstream analysis.

Differential gene expression analysis was performed in R version 4.4.1 on macOS 14.6 using the DESeq2 package version 1.46.0 [56]. A matrix containing raw counts for the remaining 11,600 genes and a corresponding metadata table were used to create the DESeq2 dataset (Table S3). Differential expression between $1,25(OH)_2D_3$ stimulation and the control group (0.1% EtOH) was assessed using the Wald test, which estimates the standard error of the $\log_2$FC to determine if it significantly differs from zero. Genes with an adjusted p-value (p_{adj}) < 0.05 were considered statistically significant.

Abbreviations

$1,25(OH)_2D_3$ or 1,25D	1α,25-Dihydroxyvitamin D_3
CAMP	Cathelicidin antimicrobial peptide
CD14	CD14 molecule
ChIP-seq	Chromatin immunoprecipitation sequencing
CPM	Counts per million
CTCF	CCCTC-binding factor
DR3	Direct repeat spaced by 3 nucleotides
FBP1	Fructose-bisphosphatase 1
FBS	Fetal bovine serum
FC	Fold change
FDR	False discovery rate
GEO	Gene expression omnibus
Hi-C	High-throughput chromosome conformation capture
HOMER	Hypergeometric Optimization of Motif EnRichment
RARA	Retinoic acid receptor alpha
RNA-seq	RNA sequencing
RXR	Retinoid X receptor
TAD	Topologically associated domain
THRB	Thyroid hormone receptor beta
TSS	Transcription start site
VDR	Vitamin D receptor

Supplementary Information

The online version contains supplementary material available at https://doi.org/10.1186/s13072-026-00677-y.

Supplementary Material 1.

Supplementary Material 2.

Supplementary Material 3.

Supplementary Material 4.

Supplementary Material 5.

Supplementary Material 6.

Supplementary Material 7.

Supplementary Material 8.

Supplementary Material 9.

Supplementary Material 10.

Supplementary Material 11.

Supplementary Material 12.

Acknowledgements

The authors gratefully acknowledge the Gene Core facility at the European Molecular Biology Laboratory (EMBL), Heidelberg, Germany, for providing high-throughput sequencing services and the Centre of Informatics Tricity Academic Supercomputer and Network of the Technical University of Gdansk (https://task.gda.pl/en) for the use of their supercomputer.

Author contributions

SS performed all experiments, while AN conducted the initial data analysis. PAF carried out all final data processing and interpretation. The manuscript was written by CC and further refined by all authors. All authors reviewed and approved the final version of the manuscript.

Funding

This publication is part of the WELCOME2 project that has received funding from the European Union's Horizon2020 research and innovation program

under grant agreement no. 952601. In addition, this work was supported by a grant from the Polish National Science Centre (Grant No. 2023/49/B/NZ9/00402) to CC.

Data availability

The raw sequencing data (FASTQ files) are available at the Gene Expression Omnibus (GEO, www.ncbi.nlm.nih.gov/geo) under accession numbers GSE308006, GSE124056, GSE89431 (ChIP-seq), and GSE69284 (RNA-seq).

Declarations

Competing interests

The authors declare no competing interests.

Received: 16 January 2026 / Accepted: 8 April 2026
Published online: 03 May 2026

References

1. Holick MF, MacLaughlin JA, Doppelt SH. Regulation of cutaneous previtamin D_3 photosynthesis in man: skin pigment is not an essential regulator. Science. 1981;211(4482):590–3.
2. Bendik I, Friedel A, Roos FF, Weber P, Eggersdorfer M. Vitamin D: a critical and essential micronutrient for human health. Front Physiol. 2014;5:248.
3. van de Peppel J, van Leeuwen JP. Vitamin D and gene networks in human osteoblasts. Front Physiol. 2014;5:137.
4. Baeke F, Takiishi T, Korf H, Gysemans C, Mathieu C. Vitamin D: modulator of the immune system. Curr Opin Pharmacol. 2010;10:482–96.
5. Martens PJ, Gysemans C, Verstuyf A, Mathieu AC. Vitamin D's effect on immune function. Nutrients. 2020;12(5):1248.
6. Bishop E, Ismailova A, Dimeloe SK, Hewison M, White JH. Vitamin D and immune regulation: antibacterial, antiviral, anti-inflammatory. JBMR Plus. 2021;5:e10405.
7. Netea MG, Joosten LA, Latz E, Mills KH, Natoli G, Stunnenberg HG, et al. Trained immunity: a program of innate immune memory in health and disease. Science. 2016;352(6284):aaf1098.
8. Verstuyf A, Carmeliet G, Bouillon R, Mathieu C. Vitamin D: a pleiotropic hormone. Kidney Int. 2010;78(2):140–5.
9. Feldman D, Krishnan AV, Swami S, Giovannucci E, Feldman BJ. The role of vitamin D in reducing cancer risk and progression. Nat Rev Cancer. 2014;14(5):342–57.
10. Carlberg C. The physiology of vitamin D-far more than calcium and bone. Front Physiol. 2014;5:335.
11. Carlberg C. Nutrigenomics of vitamin D. Nutrients. 2019;11(3):676.
12. Haussler MR, Haussler CA, Bartik L, Whitfield GK, Hsieh JC, Slater S, et al. Vitamin D receptor: molecular signaling and actions of nutritional ligands in disease prevention. Nutr Rev. 2008;66(10 Suppl 2):S98-112.
13. Whitfield GK, Dang HT, Schluter SF, Bernstein RM, Bunag T, Manzon LA, et al. Cloning of a functional vitamin D receptor from the lamprey (*Petromyzon marinus*), an ancient vertebrate lacking a calcified skeleton and teeth. Endocrinology. 2003;144(6):2704–16.
14. Evans RM, Mangelsdorf DJ. Nuclear receptors, RXR, and the big bang. Cell. 2014;157(1):255–66.
15. Chawla A, Repa JJ, Evans RM, Mangelsdorf DJ. Nuclear receptors and lipid physiology: opening the X-files. Science. 2001;294:1866–70.
16. Mangelsdorf DJ, Thummel C, Beato M, Herrlich P, Schütz G, Umesono K, et al. The nuclear receptor superfamily: the second decade. Cell. 1995;83:835–9.
17. Pike JW, Meyer MB, Watanuki M, Kim S, Zella LA, Fretz JA, et al. Perspectives on mechanisms of gene regulation by 1,25-dihydroxyvitamin D_3 and its receptor. J Steroid Biochem Mol Biol. 2007;103(3–5):389–95.
18. Heikkinen S, Väisänen S, Pehkonen P, Seuter S, Benes V, Carlberg C. Nuclear hormone 1α,25-dihydroxyvitamin D_3 elicits a genome-wide shift in the locations of VDR chromatin occupancy. Nucleic Acids Res. 2011;39(21):9181–93.
19. Tuoresmäki P, Väisänen S, Neme A, Heikkinen S, Carlberg C. Patterns of genome-wide VDR locations. PLoS ONE. 2014;9:e96105.
20. Neme A, Seuter S, Carlberg C. Selective regulation of biological processes by vitamin D based on the spatio-temporal cistrome of its receptor. Biochim Biophys Acta. 2017;1860:952–61.
21. Schräder M, Bendik I, Becker-Andre M, Carlberg C. Interaction between retinoic acid and vitamin D signaling pathways. J Biol Chem. 1993;268(24):17830–6.
22. Schräder M, Müller KM, Carlberg C. Specificity and flexibility of Vitamin D signaling.: modulation of the activation of natural Vitamin D response elements by thyroid hormone. J Biol Chem. 1994;269(8):5501–4.
23. Carlberg C, Campbell MJ. Vitamin D receptor signaling mechanisms: integrated actions of a well-defined transcription factor. Steroids. 2013;78(2):127–36.
24. GTEx-Consortium. The Genotype-Tissue Expression (GTEx) project. Nat Genet. 2013;45(6):580–5.
25. Seuter S, Virtanen JK, Nurmi T, Pihlajamaki J, Mursu J, Voutilainen S, et al. Molecular evaluation of vitamin D responsiveness of healthy young adults. J Steroid Biochem Mol Biol. 2017;174:314–21.
26. Gospodarska E, Ghosh Dastidar R, Carlberg C. Intervention approaches in studying the response to vitamin D_3 supplementation. Nutrients. 2023;15(15):3382.
27. Rastinejad F, Ollendorff V, Polikarpov I. Nuclear receptor full-length architectures: confronting myth and illusion with high resolution. Trends Biochem Sci. 2015;40(1):16–24.
28. Perissi V, Rosenfeld MG. Controlling nuclear receptors: the circular logic of cofactor cycles. Nat Rev Mol Cell Biol. 2005;6(7):542–54.
29. Maestro MA, Molnar F, Carlberg C. Vitamin D and is synthetic analogs. J Med Chem. 2019.
30. Carlberg C. Molecular endocrinology of vitamin D on the epigenome level. Mol Cell Endocrinol. 2017;453:14–21.
31. Carlberg C, Neme A. Machine learning approaches infer vitamin D signaling: critical impact of vitamin D receptor binding within topologically associated domains. J Steroid Biochem Mol Biol. 2019;185:103–9.
32. Warwick T, Schulz MH, Gilsbach R, Brandes RP, Seuter S. Nuclear receptor activation shapes spatial genome organization essential for gene expression control: lessons learned from the vitamin D receptor. Nucleic Acids Res. 2022;50(7):3745–63.
33. Yu M, Ren B. The three-dimensional organization of mammalian genomes. Annu Rev Cell Dev Biol. 2017;33:265–89.
34. Seuter S, Neme A, Carlberg C. Epigenome-wide effects of vitamin D and their impact on the transcriptome of human monocytes involve CTCF. Nucleic Acids Res. 2016;44:4090–104.
35. Warwick T, Schulz MH, Gunther S, Gilsbach R, Neme A, Carlberg C, et al. A hierarchical regulatory network analysis of the vitamin D induced transcriptome reveals novel regulators and complete VDR dependency in monocytes. Sci Rep. 2021;11(1):6518.
36. Jung I, Schmitt A, Diao Y, Lee AJ, Liu T, Yang D, et al. A compendium of promoter-centered long-range chromatin interactions in the human genome. Nat Genet. 2019;51(10):1442–9.
37. Heinz S, Benner C, Spann N, Bertolino E, Lin YC, Laslo P, et al. Simple combinations of lineage-determining transcription factors prime cis-regulatory elements required for macrophage and B cell identities. Mol Cell. 2010;38(4):576–89.
38. Seuter S, Neme A, Carlberg C. Epigenomic PU.1-VDR crosstalk modulates Vitamin D signaling. Biochim Biophys Acta. 2017;1860:405–15.
39. Nurminen V, Neme A, Seuter S, Carlberg C. The impact of the vitamin D-modulated epigenome on VDR target gene regulation. Biochim Biophys Acta. 2018;1861:697–705.
40. Rybinski M, Ghosh Dastidar R, Zawrotna N, Gospodarska E, Carlberg C. Chromatin and transcriptional dynamics underlying the immune-modulatory effects of vitamin D_3 in vivo. Sci Rep. 2025;16(1):2997.
41. Nurminen V, Seuter S, Carlberg C. Primary vitamin D target genes of human monocytes. Front Physiol. 2019;10:194.
42. Mianesaz H, Goczi L, Nagy G, Poliska S, Fadel L, Bojcsuk D, et al. Genomic regions occupied by both RARalpha and VDR are involved in the convergence and cooperation of retinoid and Vitamin D signaling pathways. Nucleic Acids Res. 2025. https://doi.org/10.1093/nar/gkaf230.
43. Eder M, Moene CJI, Dauban L, Magnitov M, Drayton J, de Haas M, et al. Functional maps of a genomic locus reveal confinement of an enhancer by its target gene. Science. 2025;389(6766):eads6552.
44. Tsuchiya S, Yamabe M, Yamaguchi Y, Kobayashi Y, Konno T, Tada K. Establishment and characterization of a human acute monocytic leukemia cell line (THP-1). Int J Cancer. 1980;26(2):171–6.
45. Seuter S, Heikkinen S, Carlberg C. Chromatin acetylation at transcription start sites and vitamin D receptor binding regions relates to effects of

1α,25-dihydroxyvitamin D_3 and histone deacetylase inhibitors on gene expression. Nucleic Acids Res. 2013;41(1):110–24.
46. Zhang J, Poh HM, Peh SQ, Sia YY, Li G, Mulawadi FH, et al. ChIA-PET analysis of transcriptional chromatin interactions. Methods. 2012;58(3):289–99.
47. Schmidl C, Rendeiro AF, Sheffield NC, Bock C. ChIPmentation: fast, robust, low-input ChIP-seq for histones and transcription factors. Nat Methods. 2015;12(10):963–5.
48. Buenrostro JD, Giresi PG, Zaba LC, Chang HY, Greenleaf WJ. Transposition of native chromatin for fast and sensitive epigenomic profiling of open chromatin, DNA-binding proteins and nucleosome position. Nat Methods. 2013;10(12):1213–8.
49. Langmead B, Trapnell C, Pop M, Salzberg SL. Ultrafast and memory-efficient alignment of short DNA sequences to the human genome. Genome Biol. 2009;10(3):R25.
50. Amemiya HM, Kundaje A, Boyle AP. The ENCODE Blacklist: identification of problematic regions of the genome. Sci Rep. 2019;9(1):9354.
51. Lun AT, Smyth GK. csaw: a Bioconductor package for differential binding analysis of ChIP-seq data using sliding windows. Nucleic Acids Res. 2016;44(5):e45.
52. Robinson MD, McCarthy DJ, Smyth GK. edgeR: a Bioconductor package for differential expression analysis of digital gene expression data. Bioinformatics. 2010;26(1):139–40.
53. Yu G, Wang LG, He QY. ChIPseeker: an R/Bioconductor package for ChIP peak annotation, comparison and visualization. Bioinformatics. 2015;31(14):2382–3.
54. Liao Y, Smyth GK, Shi W. featureCounts: an efficient general purpose program for assigning sequence reads to genomic features. Bioinformatics. 2014;30(7):923–30.
55. Durinck S, Spellman PT, Birney E, Huber W. Mapping identifiers for the integration of genomic datasets with the R/Bioconductor package biomaRt. Nat Protoc. 2009;4(8):1184–91.
56. Love MI, Huber W, Anders S. Moderated estimation of fold change and dispersion for RNA-seq data with DESeq2. Genome Biol. 2014;15(12):550.

Publisher's Note